Synthesis of Azo-Bridged Ferrocene Oligomers and a Polymer and Electrochemical and Optical Analysis of Internuclear Electronic Interactions in Their Mixed-Valence States

Masaru Kurosawa, Takuya Nankawa, Takayuki Matsuda, Kenya Kubo, Masato Kurihara, and Hiroshi Nishihara*

Department of Chemistry, School of Science, The University of Tokyo, Hongo, Tokyo 113-0033, Japan

Received June 3, 1999

New azo-bridged ferrocene trimers, Fc−Fc′−N═N−Fc (**2**) and Fc−N═N−Fc′−N═N−Fc (**3**), where Fc and Fc′ refer to (η^5-C_5H_5)Fe(η^5-C_5H_4-) and Fe(η^5-C_5H_4-)$_2$, respectively, were obtained in the reaction of a mixture of lithioferrocene and 1,1′-dilithioferrocene with N_2O. X-ray crystallography of azoferrocene (**1**) has determined that the Fe−Fe distance is 6.80 Å in the trans form. Cyclic voltammograms of **3** in aprotic solvents such as CH_2Cl_2 or THF exhibit reversible 2e$^-$ and 1e$^-$ oxidation waves, indicating that the positive charge in the monocation is localized mostly on the terminal ferrocene unit (correspondingly, Fc$^+$−N_2−Fc′−N_2−Fc) due to a strong electron-withdrawing effect of the azo group. This charge distribution in the mixed-valence state is supported by the characteristics of intervalence-transfer (IT) bands. An asymmetrical complex, **2**, undergoes a three-step 1e$^-$ oxidation, and the two mixed-valence forms can be roughly expressed as Fc$^+$−Fc′−N_2−Fc and Fc$^+$−Fc′−N_2−Fc$^+$. The redox potentials and IT band characteristics of **1**$^+$, **2**$^+$, and **2**$^{2+}$ depend markedly on the solvent. The solvent effect of the IT band on ν_{max} cannot be interpreted only by the parameters in the Marcus−Hush theory, indicating that the nature of the solvent as donor or acceptor should be taken into account in the electron-exchange process in the mixed-valence states. More donating solvent affords higher IT and LMCT energy, indicating the hole-transfer mechanism. The reaction of 1,1′-dilithioferrocene and N_2O gives a polymer composed of [-(Fc′−N═N−Fc′)$_{0.6}$-(Fc′−Fc′)$_{0.4}$-]$_n$.

Introduction

The mixed-valence states of conjugated ferrocene dimers have attracted considerable attention for decades because they are valuable examples affording intrinsic information regarding intramolecular electron-exchange reactions.[1−16] It has been shown that the chemical structure of the conjugated spacer group and its length dramatically affect the electronic interaction between the ferrocene units. Solvation effects on the electron exchange rate are also significant, and those for biferrocene and Fc−C≡C−Fc have been analyzed by Powers and Meyer,[11] by Blackbourn and Hupp,[12] and by Weaver and co-workers[13] based on the Marcus−Hush theory.[17] More general discussion based on the Hush theory of the electron-exchange mechanism for the mixed-valence complexes has appeared widely. Recently, Creutz, Newton, and Sutin have presented the theory on the relation of metal−ligand and metal−metal coupling elements,[18] and experimental support of this CNS model has been presented by Crutchley et al.[19]

On the other hand, the synthesis and physical properties of conjugated ferrocene oligomers and polymers with more than three units have also been recent topics of research.[20−22] We have reported the synthesis of oligo- and poly(1,1′-dihexylferrocenylene)s, soluble derivatives of polyferrocenylene, and their redox potentials.[23,24] The dependence of the redox potentials on the number of ferrocene units has been interpreted based on the neighboring-site interaction model[25,26] originally presented by Aoki and Chen.[27]

One of the conjugated ferrocene dimers, azoferrocene, Fc−N═N−Fc (**1**), which is an analogue of photosensitive azobenzene, has been synthesized by a few methods,[28−30] but detailed studies of the physical properties of azoferrocene and its relatives have not yet been carried out. Only the appearance of a rather strong intervalence transfer (IT) band in its monocationic form

(1) Robin, M. B.; Day, P. *Adv. Inorg. Chem. Radiochem.* **1967**, *10*, 247.
(2) (a) Cowan, D. O.; Collins, R. L.; Kaufman, F. *J. Phys. Chem.* **1971**, *75*, 2025. (b) Cowan, D. O.; Park, J.; Barber, M.; Swift, P. *Chem. Commun.* **1971**, 1444. (c) Cowan, D. O.; Candela, G. A.; Kaufman, F. *J. Am. Chem. Soc*. **1971**, *93*, 3889. (d) LeVenda, C.; Cowan, D. O.; Leitch, C.; Bechgaard, K. *J. Am. Chem. Soc.* **1974**, *96*, 6788. (e) Morrison, W. H.; Hendrickson, D. N. *Inorg. Chem.*, **1975**, *14*, 2331.
(3) (a) Iijima, S.; Saida, R.; Motoyama, I.; Sano, H. *Bull. Chem. Soc. Jpn.* **1981**, *54*, 1375. (b) Delgado-Pena, F.; Talham, D. R.; Cowan, D. O. *J. Organomet. Chem.* **1983**, *253*, C43. (c) Cohn, M. J.; Dong, T.-Y.; Hendrickson, D. N.; Geib, S. J.; Rheingold, A. L. *J. Chem. Soc., Chem. Commun.* **1985**, 1095. (d) Dong, T.-Y.; Hendrickson, D. N.; Iwai, K.; Cohn, M. J.; Rheingold, A. L.; Sano, H.; Motoyama, I.; Nakashima, S. *J. Am. Chem. Soc*. **1985**, *107*, 7996. (e) Moore, M. F.; Wilson, S. R.; Cohn, M. J.; Dong, T.-Y.; Mueller-Westerhoff, U. T.; Hendrickson, D. N. *Inorg. Chem.* **1985**, *24*, 4559. (f) Dong, T.-Y.; Kambara, T.; Hendrickson, D. N. *J. Am. Chem. Soc.* **1986**, *108*, 5857. (g) Kambara, T.; Hendrickson, D. N.; Dong, T.-Y.; Cohn, M. J. *J. Chem. Phys.* **1987**, *86*, 2362. (h) Nakashima, S.; Katada, M.; Motoyama, I.; Sano, H. *Bull. Chem. Soc. Jpn.* **1987**, *60*, 2253. (i) Kai, M.; Katada, K.; Sano, H. *Chem. Lett.* **1988**, 1523. (j) Dong, T.-Y.; Ke, T. J.; Peng, S. M.; Yeh, S. K. *Inorg. Chem.* **1989**, *28*, 2103. (k) Dong, T.-Y.; Hwang, M. Y.; Wen, Y. S. *J. Organomet. Chem.* **1990**, *391*, 377. (l) Webb, R. J.; Geib, S. J.; Staley, D. L.; Rheingold, A. L.; Hendrickson, D. N. *J. Am. Chem. Soc.* **1990**, *112*, 5031. (m) Dong, T.-Y.; Schei, C. C.; Hsu, T. L.; Lee, S. L.; Li, S. J. *Inorg. Chem.* **1991**, *30*, 2457. (n) Webb, R. J.; Dong, T.-Y.; Pierpont, C. G.; Boone, S. R.; Chadha, R. K.; Hendrickson, D. N. *J. Am. Chem. Soc.* **1991**, *113*, 4806. (o) Webb, R. J.; Hagen, P. M.; Wittebort, R. J.; Sorai, M.; Hendrickson, D. N. *Inorg. Chem.* **1992**, *31*, 1791. (p) Dong, T.-Y.; Lee, T. Y.; Lin, H. M. *J. Organomet. Chem.* **1992**, *427*, 101. (q) Dong, T.-Y.; Chang, C. K.; Huang, C. H.; Wen, Y. S.; Lee, S. L.; Chen, J. A.; Yeh, W. Y.; Yeh, A. *J. Chem. Soc., Chem. Commun.* **1992**, 526. (r) Dong, T.-Y.; Huang, C. H.; Chang, C. K.; Wen, Y. S.; Lee, S. L.; Chen, J. A.; Yeh, W. Y.; Yeh, A. *J. Am. Chem. Soc.* **1993**, *115*, 6357. (s) Dong, T.-Y.; Schei, C. C. *J. Organomet. Chem.* **1993**, *447*, 107.

10.1021/ic990646w CCC: $18.00
Published on Web 10/13/1999

Table 1. Physical Parameters of Solvents

solvent	AN[a]	DN[b]	D_{op}[c]	D_s[c]
CH_2Cl_2	20.4	0	2.12	8.93
DCE	16.7	0	2.09	10.4
NM	20.5	2.7	1.91	37.3
NB	14.8	4.4	2.42	35.6
PhCN	15.5	11.9	2.34	25.9
MeCN	18.9	14.1	1.81	36.6
acetone	12.5	17.0	1.85	21.0
THF	8.0	20.0	1.97	7.52

[a] Reference 31. [b] Reference 32. [c] Reference 33.

has been reported,[3b] whereas no crystallographic structure or redox properties of **1** or the synthesis of higher azo-bridged ferrocene oligomers have to our knowledge been available.

In this study, we have investigated the synthesis of new azo-bridged ferrocene oligomers as well as the electronic interaction between ferrocene sites in the mixed-valence states. As for **1**, the X-ray crystallographic structure was determined. The reaction of lithioferrocene, 1,1′-dilithioferrocene, and N_2O led to a polymerization and new azo-ferrocene trimers, Fc−Fc′−N═N−Fc (**2**) and Fc−N═N−Fc′−N═N−Fc (**3**), as well as a polymer composed of $[\text{-}(Fc'\text{-}Fc')_{0.4}\text{-}(Fc'\text{-}N{=}N\text{-}Fc')_{0.6}\text{-}]_n$ (**4**), which were isolated from the reaction product. For **1**, **2**, and **3**, the redox properties and spectroscopic characteristics of their mixed-valence states were examined. The effects of solvents (Table 1)[31−33] on the ν_{max} values of the IT bands of $\mathbf{1}^+$, $\mathbf{2}^+$, and $\mathbf{2}^{2+}$ are discussed based on the Marcus−Hush theory[17,34] and the CNS theory.[18]

Results and Discussion

Synthesis, Characterization, and Structure of Azo-Bridged Ferrocene Oligomers. Azo-bridged ferrocene oligomers were synthesized by a modified method of Nesmeyanov et al.[28] that involves the reaction of a mixture of lithioferrocene and 1,1′-dilithioferrocene with N_2O (Scheme 1). The mole ratio of ferrocene to BuLi used for the preparation of lithioferrocenes in THF−ether is 2:3 matching the srtoichiometry to form lithioferrocene and dilithioferrocene at 1:1 mole ratio, but these conditions should involve unreacted ferrocene judging from the results of Guillaneux and Kagan.[35] The solution of lithioferrocenes reacts with N_2O to give ferrocene oligomers soluble in chloroform.

Reaction of 1,1′-dilithioferrocene solely with N_2O gives a higher molecular weight polymer soluble in chloroform (vide infra) and insoluble polymeric products. By using silica gel column chromatography and preparative gel permeation chromatography, we have isolated ferrocene trimers with one and two azo groups, **2** and **3**, respectively, besides a known compound, azoferrocene (**1**). The compounds were characterized by ^{1}H NMR, ^{13}C NMR, IR, UV−vis, and EI-MS spectroscopy and elemental analysis.

The azo-bridged ferrocene oligomers **1**, **2**, and **3** are purple, showing characteristic bands at 533, 535, and 542 nm with ϵ = 4170, 4750, and 6790 M^{-1} cm^{-1}, respectively, in the visible spectra, as shown in Figure 1. The absorption maximum wavelength of these bands is much longer compared with the n-π* band of azobenzene and can be assigned to an MLCT band with an electron transfer from an Fe(II) d orbital to the π* orbital of the azo group. This is supported by the fact that these bands diminish with the oxidative loss of an electron from the Fe(II) center in ferrocenyl groups (vide infra). Ferrocene dimers with conjugated spacer groups are reported to have such MLCT bands: Fc−CH═CH−Fc has a band at 458 nm with ϵ = 1450 M^{-1} cm^{-1} in CH_2Cl_2,[36] and Fc−C≡C−Fc has a band at 453 nm with ϵ = 820 M^{-1} cm^{-1} in $CHCl_3$.[10a]

Azoferrocene, **1** is a known compound, but its crystallographic analysis has not been reported. In this study, we determined the X-ray structure of **1**, an ORTEP diagram of **1** is displayed in Figure 2. The configuration around the azo group is trans; the cyclopentadienyl (Cp) rings of two ferrocenyl groups and the azo group are on a plane; and the two ferrocene units are on opposite sides of the plane. The molecule therefore belongs to the C_i point group. The Fe−Fe distance is 6.80 Å. The planarity of the structure denotes the existence of strong π-conjugation to assist in the electronic interaction between the two ferrocenyl groups.

(4) (a) Dong, T.-Y.; Lee, T.-Y.; Lee, S.-H.; Lee, G.-H.; Peng, S.-M.; *Organometallics* **1994**, *13*, 2337. (b) Dong, T.-Y.; Huang, C.-H.; Chang, C.-K.; Hsieh, H.-C.; Peng, S.-M.; Lee, G.-H. *Organometallics* **1995**, *14*, 1776. (c) Dong, T.-Y.; Lee, S.-H.; Chang, C.-K.; Lin, K.-J. *J. Chem. Soc., Chem. Commun.* **1995**, 2453.
(5) Boukheddaden, K.; Linares, J.; Bousseksou, A.; Nasser, J.; Rabah, H.; Varret, F. *Chem. Phys.* **1993**, *170*, 47.
(6) Brown, G. M.; Meyer, T. J.; Cowan, D. O.; LeVanda, C.; Kaufman, F.; Roling, P. V.; M. D. *Inorg. Chem.* **1975**, *14*, 506.
(7) Delgado-Pena, F.; Talham, D. R.; Cowan, D. O. *J. Organomet. Chem.* **1983**, *253*, C43.
(8) (a) Mueller-Westerhoff, U. T.; Eilbracht, P. *J. Am. Chem. Soc.* **1972**, *94*, 9271. (b) Pittman, C. U. Jr.; Surynarayanan, B. *J. Am. Chem. Soc.* **1974**, *96*, 7916. (c) Levanda, C.; Bechgaard, K.; Cowan, D. O.; Mueller-Westerhoff, U. T.; Elbracht, P.; Candela, G. A.; Collins, R. L. *J. Am. Chem. Soc.* **1976**, *98*, 3181.
(9) (a) Nishihara, H.; Ohta, M.; K. Aramaki, *J. Chem. Soc., Faraday Trans.* **1992**, *88*, 827. (b). Sakamoto, K.; Nishihara, H.; Aramaki, K. *J. Chem. Soc., Dalton Trans.*, **1992**, 1877. (c) Nishihara, H.; Nakagawa, T.; Aramaki, K. *Electroanalysis* **1996**, *8*, 831.
(10) (a) Rosenblum, M.; Brown, N.; Papenmier, J.; Applebaum, M. *J. Organomet. Chem.* **1966**, *6*, 173. (b) Rosenblum, M.; Brawn, N. M.; Ciappenelli, D.; Tancrede, J. *J. Organomet. Chem.* **1970**, *24*, 469. (c) Lavenda, C.; Bechgaard, K.; Cowan, D. O. *J. Org. Chem.* **1976**, *41*, 2700. (d) Kramer, J. A.; Hendrickson, D. N. *Inorg. Chem.* **1980**, *19*, 3330.
(11) Powers, M. J.; Meyer, T. J. *J. Am. Chem. Soc.* **1978**, *100*, 4393.
(12) Blackbourn, R. L.; Hupp, J. T. *J. Phys. Chem.* **1990**, *94*, 1788.
(13) McManis, G. E.; Gochev, A.; Nielson, R. M.; Weaver, M. J. *J. Phys. Chem.* **1989**, *93*, 7733.
(14) (a) Atzkern, H.; Bergerat, P.; Fritz, M.; Hiermeier, J.; Hudeczek, P.; Kahn, O.; Kanellakopulos, B.; Köhler, F. H.; Ruhs, M. *Chem. Ber.* **1994**, *127*, 277. (b) Atzkern, H.; Bergerat, P.; Beruda, H.; Fritz, M.; Hiermeier, J.; Hudeczek, P.; Kahn, O.; Köhler, F. H.; Paul, M.; Weber, B. *J. Am. Chem. Soc.* **1995**, *117*, 997.
(15) Riboou, A.-C.; Launay, J.-P.; Sachtleben, M. L.; Li, H.; Spangler, C. W. *Inorg. Chem.* **1996**, *35*, 3735.
(16) Amer, S. I.; Sadler, G.; Henry, P. M.; Ferfuson, G.; Ruhl, B. L. *Inorg. Chem.* **1985**, *24*, 1517.
(17) (a) Hush, N. S. *J. Chem. Phys.* **1958**, *28*, 962. (b) Hush, N. S. *Trans. Faraday Soc.* **1961**, *57*, 557. (c) Hush, N. S. *Prog. Inorg. Chem.* **1967**, *8*, 391. (d) Hush, N. S. *Electrochem. Acta* **1968**, *13*, 1005. (e) Hush, N. S. *Chem. Phys.* **1975**, *10*, 361. (f) Hush, N. S. *Coord. Chem. Rev.* **1985**, *64*, 135.
(18) Creutz, C.; Newton, M. D.; Sutin, N. *J. Photochem. Photobiol. A: Chem.* **1994**, *82*, 47.
(19) (a) Rezvani, A. R.; Bensimon, C.; Cromp, B.; Reber, C.; Greedan, J. E.; Kondratiev, V. V.; Crutchley, R. J. *Inorg. Chem.* **1997**, *36*, 3322. (b) Evans, C. E. B.; Naklicki, M. L.; Rezvani, A. R.; White, C. A.; Kondratiev, V. V.; Crutchley, R. J. *J. Am. Chem. Soc.* **1998**, *120*, 13096.
(20) Barlow, S.; Murphy, V. J.; Evans, J. S. O.; O'Hare, D. *Organometallics* **1995**, *14*, 3461.
(21) Rulkens, R.; Lough, A. J.; Manners, I.; Lovelace, S. R.; Grant, C.; Geiger, W. E. *J. Am. Chem. Soc.* **1996**, *118*, 12683.
(22) Manners, I. *Angew. Chem., Int. Ed. Engl.* **1996**, *35*, 1602 and references therein.
(23) Hirao, T.; Kurashina, M.; Aramaki, K.; Nishihara, H. *J. Chem. Soc., Dalton Trans.* **1996**, 2929.
(24) Nishihara, H.; Hirao, T.; Aramaki, K.; Aoki, K. *Synth. Metals* **1997**, *84*, 935.
(25) Aoki, K.; Chen, J.; Nishihara, H.; Hirao, T. *J. Electroanal. Chem.* **1996**, *416*, 151.
(26) Hirao, T.; Aramaki, K.; Nishihara, H. *Bull. Chem. Soc. Jpn.* **1998**, *71*, 1817.

Scheme 1

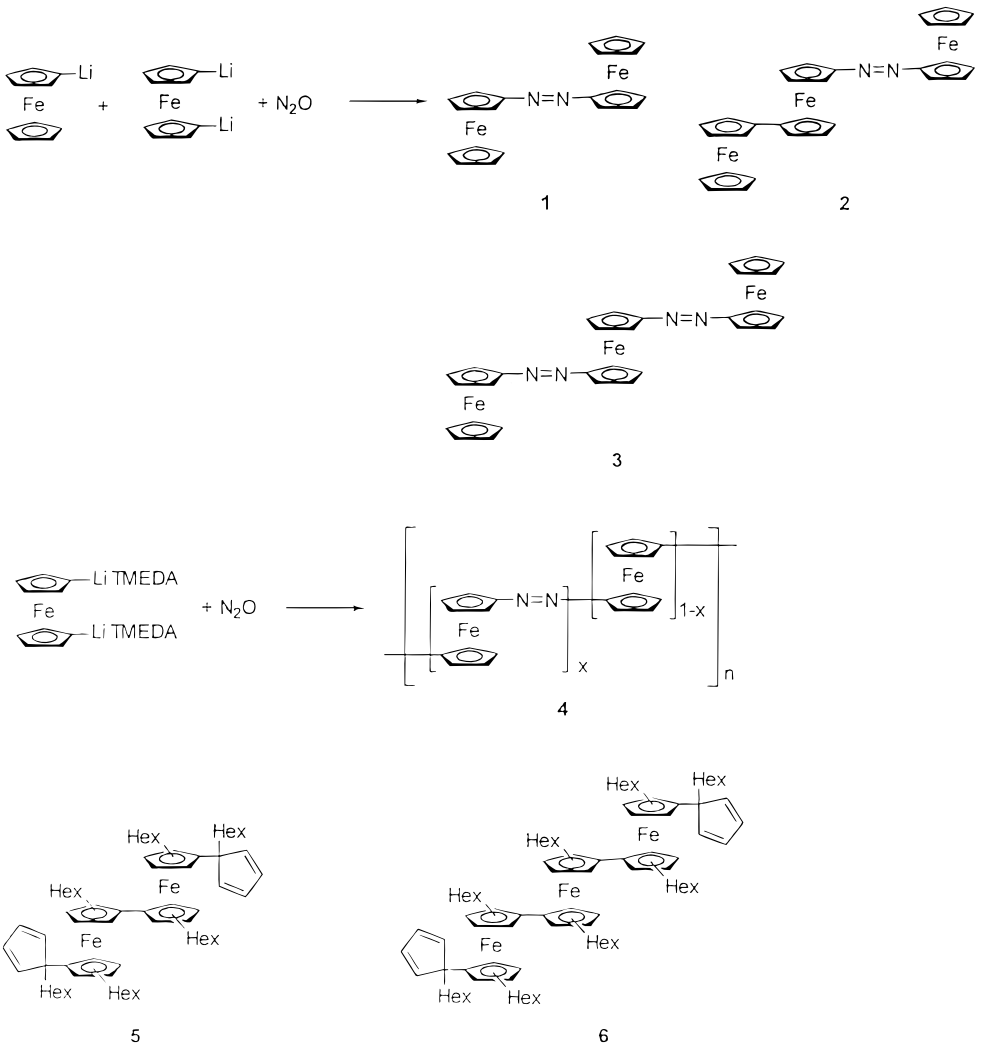

Similarity in the UV−vis spectra between **1** and trimers, **2** and **3** strongly suggests that both trimers would have the same structural characteristics as **1** such as a trans configuration around the azo group(s), a high planarity of the Cp rings, and the ferrocene units located opposite from each other against the plane(s).

Electrochemical Properties. Cyclic voltammograms and Osteryoung square-wave voltammograms for the oxidation of **1**, **2**, and **3** in 0.1 M $Bu_4NClO_4-CH_2Cl_2$ are displayed in Figure 3, and the $E^{\circ\prime}$ values are given in Table 2. Azoferrocene **1** gives reversible two $1e^-$ oxidation waves via the formation of a mixed-valence cation, and the asymmetrical trimer, **2**, undergoes a reversible three-step $1e^-$ oxidation. Considering the strong electron-withdrawing effect of the azo group, the oxidation pathway is expected to involve two mixed-valence states in which the charge distribution is roughly expressed as $Fc^+-Fc'-N_2-Fc$ and $Fc^+-Fc'-N_2-Fc^+$ as monovalent and divalent cations, respectively. This is reasonable because the first and second redox potential values of **2** are similar to those of biferrocene, and the second and third ones to those of azoferrocene.

The symmetric trimer, **3**, gives two oxidation waves for which the number of electrons are two and one in 0.1 M $Bu_4NClO_4-CH_2Cl_2$, as shown in Figure 3c. This behavior implies that the thermodynamic instability of the monocationic form of **3** is in contrast with the redox properties of terferrocene, which undergoes a three-step $1e^-$ oxidation at distinctly separate potentials.[6,23]

The redox processes of oligoferrocenylene have been interpreted by the theory based on neighboring-site interaction energies, u_{OR}, u_{OO}, and u_{RR} denoting the energy between the reduced site (Red) and the oxidized site (Ox), between Red and Red and between Ox and Ox, respectively, proposed by Aoki et al.[24−27] The parameters, u_{OR} and u_{OO} mainly consist of resonance exchange energy and electrostatic repulsion energy, respectively, in the case of azo-bridged ferrocene oligomers when the internuclear electronic interaction is strong and the

(27) Aoki, K.; Chen, J. *J. Electroanal. Chem.* **1995**, *380*, 35.
(28) Nesmeyanov, A. N.; Perevalova, E. G.; Nikitina, T. V. *Dokl. Adad. Nauk SSSR* **1961**, *138*, 118.
(29) Nesmeyanov, A. N.; Sazonova, V. A.; Romanenko, V. I. *Dokl. Adad. Nauk SSSR* **1961**, *157*, 922.
(30) Abramovitch, R. A.; Azogu, C. I.; Sutherland, R. G. *Chem. Commun*. **1971**, 134.
(31) Mayer, U.; Gutmann, V.; Gerger, W. *Monat. Chem.* **1975**, *106*, 1235.
(32) Gutmann, V. *The Donor−Acceptor Approach to Molecular Interactions*; Plenum: New York, 1978.
(33) *CRC Handbook of Chemistry and Physics*, 79th ed.; Lide, D. R., Ed.; CRC Press: Boca Raton, FL, 1998.
(34) Marcus, R. A. *J. Chem. Phys.* **1965**, *45*, 679.
(35) Guillaneux, D.; Kagan, H. B. *J. Org. Chem.* **1995**, *60*, 2502.
(36) Ribou, A. C.; Launay, J. P.; Sachtleben, M. L.; Li, H.; Spangler, C. W. *Inorg. Chem.* **1996**, *35*, 3735.

Table 2. Redox Properties of Azo-Bridged Ferrocene Oligomers

		$E^{\circ\prime}/V^a$						
complex	solvent	1st	2nd	3rd	$\Delta E^{\circ\prime}_{12}$ (V)	$\Delta E^{\circ\prime}_{23}$ (V)	log K_{c1}	log K_{c2}
1	CH_2Cl_2[b]	0.106	0.316	−	0.210	−	3.56	−
	CH_2Cl_2	0.090	0.320	−	0.230	−	3.90	−
	DCE	0.080	0.318	−	0.238	−	4.03	−
	NM	0.068	0.334	−	0.266	−	4.51	−
	NB	0.105	0.329	−	0.224	−	3.80	−
	PhCN	0.101	0.318	−	0.217	−	3.68	−
	MeCN	0.119	0.331	−	0.212	−	3.59	−
	acetone	0.063	0.266	−	0.203	−	3.44	−
	THF	0.088	0.263	−	0.175	−	2.97	−
2	CH_2Cl_2[b]	−0.054	0.156	0.476	0.210	0.370	3.56	6.27
	CH_2Cl_2	−0.073	0.144	0.514	0.217	0.370	3.68	6.27
	DCE	−0.088	0.132	0.495	0.220	0.363	3.73	6.15
	NM	−0.046	0.176	0.515	0.221	0.339	3.75	5.75
	NB	−0.062	0.150	0.485	0.212	0.335	3.59	5.68
	PhCN	−0.065	0.213	0.523	0.213	0.310	3.61	5.25
	MeCN	−0.043	0.155	0.495	0.198	0.340	3.36	5.76
	acetone	−0.101	0.098	0.412	0.199	0.314	3.37	5.32
	THF	−0.078	0.090	0.392	0.168	0.302	2.85	5.12
3	CH_2Cl_2[b]	0.136 ($2e^-$)		0.526	−	0.390	−	6.61
	CH_2Cl_2	0.092	0.173	0.551	0.081	0.378	1.37	6.41
	THF	0.102 ($2e^-$)		0.484	−	0.382	−	6.47

[a] Versus ferrocene/ferrocenium at 25 °C. [b] Added 0.1 M Bu_4NClO_4. Other solutions contained 0.1 M Bu_4NPF_6.

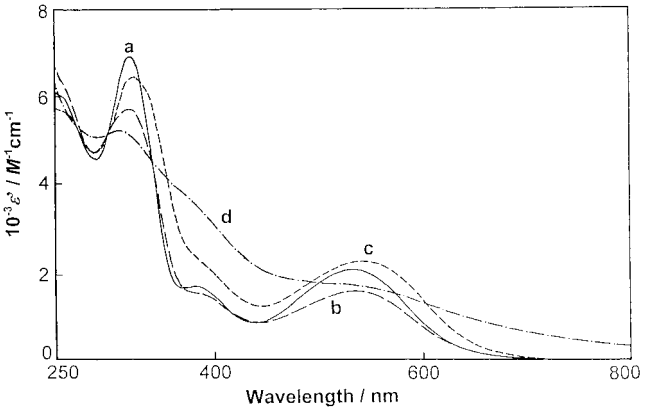

Figure 1. UV−vis absorption spectra of **1**, **2**, **3**, and **4** for a, b, c, and d, respectively, in CH_2Cl_2. The ϵ' value is the quotient of ϵ divided by the number of ferrocene units in a molecule.

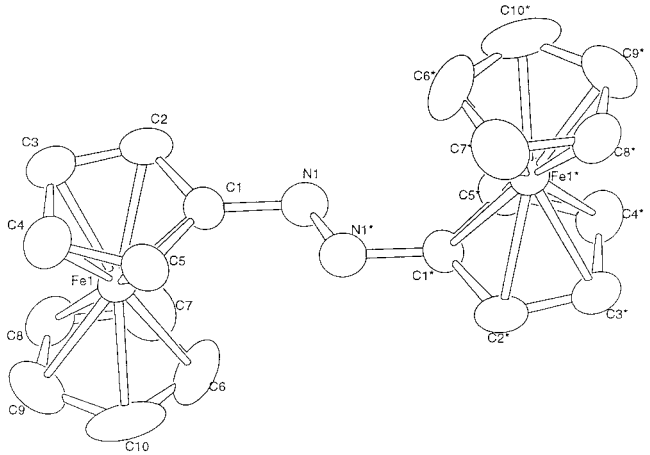

Figure 2. ORTEP drawing of **1** with a probability level of 50%. Selected bond length (Å) and angles (deg): Fe1−C1, 2.039(8); Fe1−C2, 2.059(8); Fe1−C3, 2.072(10); Fe1−C4, 2.06(1); Fe1−C5, 2.050(8); Fe1−C6, 2.05(1); Fe1−C7, 2.06(1); Fe1−C8, 2.041(9); Fe1−C9, 2.031(10); Fe1−C10, 2.025(10); C1−N1, 1.43(1); N1−N1*, 1.27(1); C2−C1−N1, 120.8(7); C5−C1−N1, 129.8(8); C1−N1−N1*, 111.4(9).

oxidized site is positively charged. This simple approach has been effective for considering the redox properties of multinuclear complexes,[24,25] while more strict analysis on the free energy of comproportionation has been presented for dinuclear complexes.[19b,37]

Using the neighboring-site interaction theory, Fc−Fc′$^+$−Fc is more thermodynamically favorable than Fc$^+$−Fc−Fc because of the larger attractive interactions between the reduced and oxidized units, and three-step $1e^-$ waves should appear (see Table 3, part A, Fc−Fc′$^+$−Fc corresponds to Red-Ox-Red). This model holds based on the assumption that the electrochemical potential of the central ferrocene unit is similar to that of the terminal ferrocene unit. However, in the case of azo-bridged ferrocene oligomers, the strong electron-withdrawing effects of the azo group on the electrochemical potentials of the ferrocene units are significant, as has been seen in the redox potentials of **1** and **2**. Thus, a likely interpretation of the electrochemical results for **3** is that the thermodynamically favorable form of its monocation is not Fc−N_2−Fc′$^+$−N_2−Fc but Fc$^+$−N_2−Fc′−N_2−Fc. Actually, the consideration based on the neighboring site interaction energies on the oxidation process involving Fc$^+$−N_2−Fc′−N_2−Fc and Fc$^+$−N_2−Fc′−N_2−Fc$^+$ shows no difference in the potentials of the first and second electron-transfer steps, resulting in an apparent simultaneous $2e^-$ transfer reaction as shown in Table 3, part B (Ox^1-Red^2-Red^1 and Ox^1-Red^2-Ox^1 correspond to Fc$^+$−N_2−Fc′−N_2−Fc and Fc$^+$−N_2−Fc′−N_2−Fc$^+$, respectively, and the second neighboring site interaction energy, u_{OXR} (see below), is negligible in this case). It should be emphasized that the $2e^- + 1e^-$ redox process occurs for trinuclear complexes even if the internuclear electronic interaction is significant as **3** as proved by the appearance of strong IT bands (vide infra).

The cyclic voltammogram of **3** in 0.1 M Bu_4NPF_6−CH_2Cl_2 also exhibits $2e^-$ and $1e^-$ oxidation waves in a rough sense. However, the first wave is broader than that in the solution with ClO_4^- as the electrolyte anion, as shown in Figure 4. Digital simulation of the first $2e^-$ wave in the cyclic voltammograms

(37) Sutton, J. E.; Sutton, P. M.; Taube, H. *Inorg. Chem.* **1979**, *18*, 1017.

Table 3. Redox Potentials, E_i, and Their Differences, $\Delta E_{i(i+1)}$ for Trimers Composed of Equivalent (A) and Nonequivalent Redox Sites (B) Based on Site-to-site Interaction Energy, U_i[a]

oxidation state	$\mu_i + U_i$	E_i ($i = 1, 2, 3$)	$\Delta E_{i(i+1)}$ ($i = 1, 2$)
(A)			
Red-Red-Red	$3\mu_R + 2u_{RR}$		
Red-Ox-Red	$2\mu_R + \mu_O + 2u_{OR}$	$\mu_O - \mu_R + 2(u_{OR} - u_{RR})$	$2(u_{RR} - u_{OR})$
Ox-Red-Ox	$\mu_R + 2\mu_O + 2u_{OR}$	$\mu_O - \mu_R$	$2(u_{OO} - u_{OR})$
Ox-Ox-Ox	$3\mu_O + 2u_{OO}$	$\mu_O - \mu_R + 2(u_{OO} - u_{OR})$	
(B)			
Red^1-Red^2-Red^1	$2\mu_{R1} + \mu_{R2} + 2u_{R1R2}$		
Ox^1-Red^2-Red^1	$\mu_{R1} + \mu_{R2} + \mu_{O1} + u_{R1R2} + u_{O1R2} + (u_{O1XR1})$	$\mu_{O1} - \mu_{R1} + u_{O1R2} - u_{R1R2} + (u_{O1XR1})$	$(-2u_{O1XR1})$[b]
Ox^1-Red^2-Ox^1	$\mu_{R2} + 2\mu_{O1} + 2u_{O1R2}$	$\mu_{O1} - \mu_{R1} + u_{O1R2} - u_{R1R2} - (u_{O1XR1})$	$\mu_{O2} - \mu_{R2} - \mu_{O1} + \mu_{R1} + 2u_{O1O2} - 3u_{O1R2} + u_{R1R2} + (u_{O1XR1})$
Ox^1-Ox^2-Ox^1	$2\mu_{O1} + \mu_{O2} + 2u_{O1O2}$	$\mu_{O2} - \mu_{R2} + 2(u_{O1O2} - u_{O1R2})$	

[a] u_{OR}, u_{RR}, and u_{OO} denote the neighboring site interaction energy between the reduced site (Red) and oxidized site (Ox), between Red and Red, and between Ox and Ox, respectively. [b] u_{OXR} indicates the second-neighboring site interaction energy between Ox and Red, which is neglected when only the first-neighboring site interaction is taken into account.

in solutions with ClO_4^- and PF_6^- shows small differences in the redox potentials between successive $1e^-$ steps, $\Delta E^{\circ\prime}_{12}$ as 65 and 81 mV, respectively. This is not contradictory to the position described above suggesting that the oxidation process involving $Fc^+-N_2-Fc'-N_2-Fc$ gives $\Delta E^{\circ\prime}_{12} = 0$, because such small differences as 65−81 mV cannot be explained by the process involving $Fc-N_2-Fc'^+-N_2-Fc$.[38] A possible cause for the generation of such a small $\Delta E^{\circ\prime}_{12}$ is the second neighboring site interaction between Red and Ox (whether the central unit is Red or Ox). The introduction of the second neighboring site interaction energy, u_{OXR} (3.8 kJ mol^{-1}), actually makes it possible to simulate the experimentally obtained $E^{\circ\prime}$ values for oligoferrocenylene up to the heptamer.[24,25] In the present case of **3** involving Ox^1-Red^2-Red^1 and Ox^1-Red^2-Ox^1 as mixed-valence states, the $\Delta E^{\circ\prime}_{12}$ value corresponds to $-2u_{O1XR1}$ (see Table 3, part B). The u_{O1XR1} values evaluated from $\Delta E^{\circ\prime}_{12} =$ 65 and 81 mV for ClO_4^- and PF_6^- are 3.1 and 3.9 kJ mol^{-1}, which are comparable to the 3.8 kJ mol^{-1} of oligoferrocenylene, and thus fairly reasonable. The comproportionation constant, K_c for $\mathbf{3}^\circ + \mathbf{3}^{2+} \leftrightarrow 2 \times \mathbf{3}^+$ estimated from $\Delta E^{\circ\prime}_{12} = 65$ and 81 mV is 13 and 23, indicating that 64% and 72% of $\mathbf{3}^+$ exist at $(1/2)(E^{\circ\prime}_2 - E^{\circ\prime}_1)$ in $Bu_4NClO_4-CH_2Cl_2$ and $Bu_4NPF_6-CH_2Cl_2$, respectively.

Cyclic voltammetry for the reduction of **1** and **2** with a single azo group in 0.1 M Bu_4NPF_6−THF shows a quasi-reversible $1e^-$ reduction wave at $E^{\circ\prime} = -2.32$ and -2.34 V vs ferrocene/ferrocenium due to the reduction of an azo group similar to azobenzene.[39] In contrast, **3** with two azo groups exhibits two irreversible reduction waves at $E_p = -2.26$ and -2.41 V vs ferrocene/ferrocenium, suggesting two successive $1e^-$ reduction steps and thus the existence of electronic communication between the two azo groups via the central ferrocene unit.

Intervalence-Transfer Bands. Vis−NIR absorption spectra of the oxidized forms of **1**, **2**, and **3** were observed by adding a given amount of oxidant, $[Fe(\eta^5\text{-}C_5H_4Cl)_2]PF_6$, of which $E^{\circ\prime}$ is 0.258 V vs ferrocene/ferrocenium for their solutions in CH_2Cl_2, and the results are given in Figure 5. It should be noted that Delgado-Pena et al. have reported that the IT band of $\mathbf{1}^+$ appears at $\lambda_{max} = 1760$ nm in 0.2 M $Bu_4NBF_4-CH_2Cl_2$.[3b] In Figure 5a, an intervalence-transfer (IT) band of $\mathbf{1}^+$ appears at $\lambda_{max} = 2036$ nm, which reaches a maximum intensity when the mole ratio of **1** to the oxidant is 1:1, as expected. The absorption of the MLCT band at 534 nm diminishes and a new band appears and increases at 672 nm with the oxidation to $\mathbf{1}^+$. The new band can be assigned to an LMCT band with an electron transfer from the π orbital of the azo group to an Fe(III) d orbital. The asymmetric trimer **2** shows two-step changes, as seen in Figure 5b. The absorption peaks at 2039 nm and at 1456 nm reach a maximum intensity at mole ratios of **2** to the oxidant of 1:1 and 1:2, respectively, corresponding to the formation of

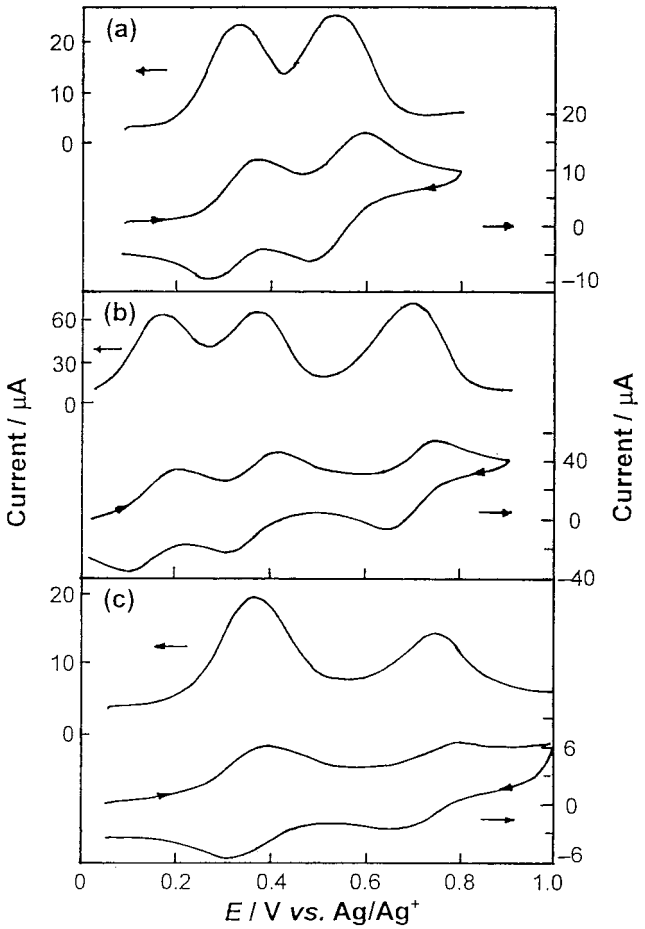

Figure 3. Cyclic voltammograms (scan rate: 0.1 V s^{-1}) and Osteryoung square-wave voltammograms (frequency, 15 Hz; potential step, 4 mV) of **1** (a), **2** (b), and **3** (c) at GC in 0.1 M $Bu_4NClO_4-CH_2Cl_2$.

(38) For example, $2(u_{RR} - u_{OR}) = 65$ mV and $2(u_{OO} - u_{OR}) = 357$ mV gives $u_{OR} = -33$ mV and $u_{OO} = 146$ mV assuming $u_{RR} = 0$. This is not reasonable since $u_{OR} = -110$ mV and $u_{OO} = 80$ mV assuming $u_{RR} = 0$ for terferrocene and u_{OO} for the longer distance between the charged sites $Fc^+-N_2-Fc^+$ should be smaller than that for the shorter distance, Fc^+-Fc^+.

(39) Bard, A. J.; Faulkner, L. R. *Electrochemical Methods. Fundamentals and Applications*; Wiley: New York, 1980; p 701.

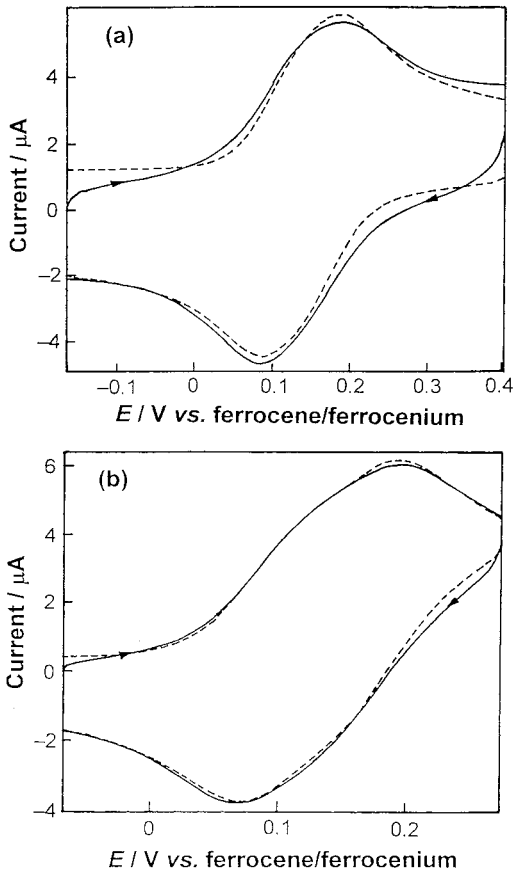

Figure 4. Cyclic voltammogram of **3** at GC at 0.1 V s^{-1} at 25 °C in 0.1 M $Bu_4NClO_4-CH_2Cl_2$ (a) and in 0.1 M $Bu_4NPF_6-CH_2Cl_2$ (b) as solid lines and their simulated voltammograms on the boundary finite diffusion model as broken lines. Values of finite diffusion layer thickness, C_{dl}, $E^{o'}_1$, α_1, k_{s1}, $E^{o'}_2$, α_2, k_{s2}, D_R, D_O, and R used for the simulation are 0.415 mm, 12 μF, 0.320 V, 0.6, 1.0×10^4 cm s^{-1}, 0.385 V, 0.6, 1.0×10^4 cm s^{-1}, 1.0×10^5 cm^2 s^{-1}, 1.0×10^5 cm^2 s^{-1}, and 500 Ω for a and 0.415 mm, 4.2 μF, 0.314 V, 0.5, 1.0×10^4 cm s^{-1}, 0.395 V, 0.5, 1.0×10^4 cm s^{-1}, 1.0×10^5 cm^2 s^{-1}, 1.0×10^5 cm^2 s^{-1}, and 500 Ω for b, respectively.

two mixed-valence states, $\mathbf{2}^+$ and $\mathbf{2}^{2+}$. The absorption at 535 nm due to MLCT does not change significantly at $\mathbf{2}^+$ and disappears at $\mathbf{2}^{2+}$. This is consistent with our conviction based on the redox behaviors that the $\mathbf{2}^+$ charge is primarily located on the terminal ferrocene unit nonadjacent to the azo group so that the d-π* transition is not as greatly influenced. The LMCT band appears at 630 and 652 nm for $\mathbf{2}^+$ and $\mathbf{2}^{2+}$, respectively. The symmetric trimer, **3** also gives two-step changes, and IT bands appear at λ_{max} = 1778 and 1340 nm for $\mathbf{3}^+$ and $\mathbf{3}^{2+}$, respectively, as shown in Figure 5c. In this case, the MLCT band decreases significantly in the first oxidation step and further in the second step. This is reasonable because both of the terminal ferrocene groups are adjacent to the azo groups. The LMCT band appearing at 678 nm for $\mathbf{3}^+$ shifts to a shorter wavelength, 668 nm for $\mathbf{3}^{2+}$.

Table 4 presents the absorption maximum wavenumbers, ν_{max}, the molar absorption coefficient, ϵ_{max} and the half-height bandwidth, $\Delta\nu_{1/2}$ for the IT bands and ν_{max} and ϵ_{max} for the LMCT bands of the mixed-valence states of **1**, **2**, and **3**. Data for $\mathbf{3}^+$ were obtained considering the low K_c value as noted above. It should be noted that ν_{max} and ϵ_{max} are confident but some error in $\Delta\nu_{1/2}$ (ca. 10%) may exist because of the broadness of the IT band and overlapping of the strong LMCT band. The mixing coefficient, α, and the off-diagonal matrix-coupling element in the Marcus−Hush two-state model, H_{AB}, of $\mathbf{1}^+$ in CH_2Cl_2 are evaluated to be 0.057 and 280 cm^{-1}, respectively, using eqs 1 and 2 and an Fe−Fe distance, r, of 6.80 Å.[40]

$$\alpha^2 = (4.2 \times 10^{-4})\epsilon_{max}\Delta\nu_{1/2}\nu_{max} - 1r^{-2} \quad (1)$$

$$H_{AB} = \nu_{max}\alpha \quad (2)$$

It is valuable to compare the characteristics of the IT bands between **3** and terferrocenylene as their redox processes are different as discussed above. As for ter(1,1′-dihexylferrocene) (**5**), ν_{max}, ϵ_{max}, and $\Delta\nu_{1/2}$ for the 1+ ion are 4830 cm^{-1}, 1490 M^{-1} cm^{-1}, and 3130 cm^{-1}, and those for the 2+ ion are 6140 cm^{-1}, 990 M^{-1} cm^{-1}, and 3330 cm^{-1}, respectively, in CH_2Cl_2−acetone.[41] Comparison of these values with those of **3** shows different behaviors; the ν_{max} and ϵ_{max} values are slightly lower for $\mathbf{5}^{2+}$ than $\mathbf{5}^+$, but both values are higher for $\mathbf{3}^{2+}$ than $\mathbf{3}^+$. This can be attributed to the difference in the electronic structure of the mixed-valence states between **3** and **5**. The charge localization of $\mathbf{3}^+$ and $\mathbf{3}^{2+}$ has u_{OR} and $2u_{OR}$, respectively, whereas both $\mathbf{5}^+$ and $\mathbf{5}^{2+}$ have $2u_{OR}$ (Table 3).[25] The smaller interaction energy in $\mathbf{3}^+$ corresponds well to the smaller $\epsilon_{max}\nu_{max}\Delta\nu_{1/2}$ compared to that of $\mathbf{3}^{2+}$.

Solvent Effects on the Internuclear Interaction. Tables 2 and 4 exhibit the electrochemical and spectroscopic results for **1**, **2**, and **3** in several solutions. Considerable solvent effects are seen on both the redox potential differences, $\Delta E^{o'}$, and ν_{max} of the IT bands. Figure 6 displays plots of $\Delta E^{o'}$ vs acceptor number (AN) and donor number (DN) of the solvents for **1** and **2**. There appear to be significant correlation, denoting that the more accepting or less donating solvent is effective for the thermodynamic stabilization of mixed-valence states. The correlation is higher in the plots of $\Delta E^{o'}$ vs AN−DN compared to those vs either AN or DN.

As ΔE_{12} is expressed using neighboring-site interaction energies of $u_{RR} + u_{OO} - 2u_{OR}$, we consider the solvent effects on both u_{OR} and u_{OO}. The stronger solvation of donating solvents to the cationic center of the ferrocenium site causes a localization of charge, leading to a lessening of the internuclear electron-exchange stabilization. In contrast, accepting solvents strongly solvate the counteranion and decrease the Coulombic interaction between the ferrocenium site and the counterion, resulting in an enhancement of the charge delocalization in the mixed-valence states. Consequently, u_{OR}, usually a negative value, would decrease in solvents with smaller DN and/or larger AN. However, correlation between H_{AB} and AN−DN is insignificant in Table 4, suggesting that the contribution of the charge delocalization is not the major factor of the $\Delta E^{o'}$ vs AN−DN relationship. The u_{OO} would be smaller in the solvent with higher DN because the solvation to the ferrocenium sites decreases the Coulombic repulsion of the two cationic centers. Solvent with larger AN solvates to the counteranion, causing an increase in the Coulombic repulion. These solvent effects on u_{OO} are coincident with the dependence of $\Delta E^{o'}$ on AN−DN.

Solvent effects on ν_{max} of the IT band have been discussed in relation to the Marcus−Hush theory as given in eqs 3−5,

(40) Delgado-Pena et al. have reported that $\alpha = 0.05$ in 0.2 M $Bu_4NBF_4-CH_2Cl_2$ in ref 3b.

(41) Nishihara, H.; Horikoshi, T. *Synth. Metals* **1999**, *102*, 1523. The solvent used for **5** is different from the one for **3**, CH_2Cl_2 or THF, but qualitative discussion on the difference in the parameters of IT bands between 1+ and 2+ ions can be made because it does not depend on the solvent for a given complex (compare $\mathbf{2}^+$ vs $\mathbf{2}^{2+}$ or $\mathbf{3}^+$ vs $\mathbf{3}^{2+}$ in Table 4).

$$E_{op} = \nu_{max} = 4\Delta G_{th}^{\ddagger} \quad (3)$$

$$\Delta G_{th}^{\ddagger} = \Delta G_{in}^{\ddagger} + \Delta G_{out}^{\ddagger} \quad (4)$$

$$\Delta G_{out}^{\ddagger} = (e^2/4)(^1/_2 a_1 + {}^1/_2 a_2 - 1/r)(1/D_{op} - 1/D_s) \quad (5)$$

where $\Delta G_{th}^{\ddagger}$, $\Delta G_{in}^{\ddagger}$, $\Delta G_{out}^{\ddagger}$, a_1, a_2, r, D_{op}, and D_s are the total activation energy for the thermal electron exchange process, the inner-sphere and outer-sphere components of the activation energy, the radii of the two redox nuclei, the distance between the nuclei, and the solvent's optical and static dielectric constants, respectively. Powers and Meyer,[11] Blackbourn and Hupp,[12] and Weaver et al.[13] have reported a linear relationship of ν_{max} on $(1/D_{op} - 1/D_s)$ for Fc−C≡C−Fc and have emphasized the usefulness of the Marcus−Hush relationship. We plot the relation of ν_{max} vs $(1/D_{op} - 1/D_s)$ for $\mathbf{1}^+$ and $\mathbf{2}^+$ in Figure 7a. In this figure, however, no acceptable correlation is observed. The solvents used in our experiments are MeCN, acetone, nitromethane (NM), nitrobenzene (NB), PhCN, CH_2Cl_2, THF, and 1,2-dichloroehtane (DCE), among which THF and DCE were not used in the reports for Fc−C≡C−Fc$^+$. Plots for the other six solvents common to both their and our experiments show a quite similar tendency between Fc−C≡C−Fc$^+$ and $\mathbf{1}^+$. This implies that the addition of the plots for THF and DCE lose the correlation between ν_{max} and $(1/D_{op} - 1/D_s)$ shown in Figure 7a. It should be noted that the low ν_{max} values of Fc−C≡C−Fc$^+$ in CH_2Cl_2 has been discussed based on the ion-pairing and dielectric saturation effects in the previous studies.[12,13]

The ν_{max} value of $\mathbf{1}^+$ in Table 4 is 80−90% of that for Fc−C≡C−Fc$^+$ [11] in each solvent. This is inexplicable by the dielectric continuum theory[13] in which the nature of bridge is not supposed to count in determining the inner and outer reorganizational parameters, λ_i and λ_o. By the theory, $\nu_{max} = \lambda_i + \lambda_o$ should be similar for the systems with alike Fe−Fe distances as $\mathbf{1}^+$ and Fc−C≡C−Fc$^+$.

As the $\Delta E^{\circ\prime}$ values are significantly dependent on DN and/or AN, we added these parameters to the plot of ν_{max}, and the results for $\mathbf{1}^+$ are shown in Figure 7b. The parameter AN−DN does not afford a nice correlation by itself, nor does $(1/D_{op} - 1/D_s)$, but the combination of $(1/D_{op} - 1/D_s)$ and AN−DN gives a fairly good correlation with ν_{max}.[42] The significant contribution of DN and/or AN indicates that the coordination character of the solvent is important for the internuclear electron exchange process in addition to the dipole reorganization characteristics. The coordination of the solvent to the redox center would perturb the intrinsic structure around the center and thus might contribute to the inner-sphere term, $\Delta G_{in}^{\ddagger}$. Similar DN effects have been reported for $Ru^{II}Ru^{III}$ polyamine mixed-valence complexes, for which the effect has been interpreted by the redox-state-dependent rearrangements of hydrogen bonds between solvent and solute in the second coordination sphere by Curtis et al.,[43] and solvent−ammine donor−acceptor interactions by Crutchley et al.[19b]

The monocationic form of a trimer, $\mathbf{2}^+$ also gives a correlation between ν_{max} vs $150(1/D_{op} - 1/D_s) - (AN-DN)$ (Figure 7b), whereas the plots for the dication $\mathbf{2}^{2+}$ show two points beside the correlation (Figure 7c). They are the plots for MeCN and PhCN. It has been determined that the ferrocene derivative [Fe(η^5,η^5-$C_5Me_4(CH_2)_3C_5Me_4$)$_2$] undergoes an ECE reaction in MeCN, forming a divalent cation in which MeCN coordinates to the iron center.[44] In the trimer **2**, the terminal ferrocene unit with no neighboring azo group is much more facile at being oxidized than the others, so that the dicationic form $\mathbf{2}^{2+}$ may be capable of contributing (RCN)Fc^{2+}−Fc′−N_2−Fc in addition to the original structure Fc$^+$−Fc−N_2−Fc$^+$ due to the strong coordination ability of nitriles. This is a possible reason for the peculiar plots shown in Figure 7c.

Crutchley and co-workers have presented that the solvent dependency of superexchange in $Ru^{II}Ru^{III}$ complexes is interpretable by the hole-transfer mechanism based on the CNS model.[19b] As for the azo-bridged ferrocene oligomers in this study, solvent does not affect ν_{max} of the MLCT band in the neutral form but does the LMCT band in the mixed-valence states as seen in Table 4. Plots of ν_{max}(IT) vs ν_{max}(LMCT) is displayed in Figure 8,[45] indicating positive relationship for all the mixed-valence states of **1**−**3**. This connotes the strong assistance of superexchange between Fe(II) and Fe(III) by the bridging ligand in the hole-transfer mechanism.

Synthesis and Physical Properties of an Azo-Bridged Ferrocene Polymer (4). Synthesis of azo-bridged ferrocene polymer was attempted through the reaction of 1,1′-dilithioferrocene and N_2O under high-pressure conditions (40 kgw/cm^2).[46] The product contained insoluble and soluble components in chloroform, and the soluble component was separated from low molecular weight products by preparative GPC and purified by reprecipitation from chloroform−acetonitrile. The average molecular weight of the polymer **4** is $M_w = 8.7 \times 10^4$ and $M_n = 1.3 \times 10^4$. The elemental analysis data indicate that the contents of azo-bridged ferrocene units and directly connected ferrocene units are ca. 60% and ca. 40%, respectively. The UV−vis absorption spectrum in chloroform shows an MLCT band at 535 nm, and the $\pi-\pi^*$ band edge shifts to a longer wavelength, probably due to the elongation of the π-conjugation (see Figure 1).

Cyclic voltammetry of **4** dissolved in $Bu_4NClO_4-CH_2Cl_2$ was carried out, and the result is shown in Figure 9. A chemically quasi-reversible broad redox wave appears, and the $E^{\circ\prime}$ value estimated from the maximum peak potentials is 0.32 V vs Ag/Ag$^+$ (0.11 V vs ferrocene/ferrocenium). This is between the average values of the redox potentials for azo-bridged ferrocene oligomers such as **1** or **3** and those for directly connected ones such as biferrocene or terferrocene.

A spin-coated film of **4** also gives a broad redox wave with $E^{\circ\prime} = 0.26$ V vs Ag/Ag$^+$ in Bu_4NClO_4−MeCN (Figure 10a). Spectral changes of the film with a potential shift in the positive direction indicate a decrease in intensity of the MLCT band and the appearance of a broad IT band around 1000 nm at 0.25 V, generating the mixed-valence state Bu_4NClO_4−MeCN (Figure 10b). A further decrease in the intensity of the MLCT band and the disappearance of the IT band represents the formation of the fully oxidized state at 0.8 V.

Experimental Section

General Methods. 1,1′-Dichloroferrocenium hexafluorophosphate was prepared by the oxidation of 1,1′-dichloroferrocene[26] with sulfuric

(42) The adjusting parameter expressing the ratio of $(1/D_{op} - 1/D_s)$ to AN−DN affording the best correlation is 150, but this value is not meaningful because DN and AN are relative parameters.

(43) Mao, W.; Qian, Z.; Yen, H.-J.; Crutis, J. C. *J. Am. Chem. Soc.* **1996**, *118*, 3247.

(44) Ogino, H.; Tobita, H.; Habazaki, H.; Shimoi, M. *J. Chem. Soc., Chem. Commun*. **1989**, 828.

(45) Plots for $\mathbf{2}^{2+}$ in PhCN and MeCN are omitted in Figure 8 because of the peculiar behavior of $\mathbf{2}^{2+}$ in such solvents as discussed in the text.

(46) For conjugated ferrocene polymers, see for example: Nishihara, H. Organometallic Conductive Polymers. In *Handbook of Organic Conductive Molecules and Polymers*; Nalwa, H. S., Ed.; Wiley: New York, 1997; Vol. 2, Chapter 19, pp 799−832, and the references therein.

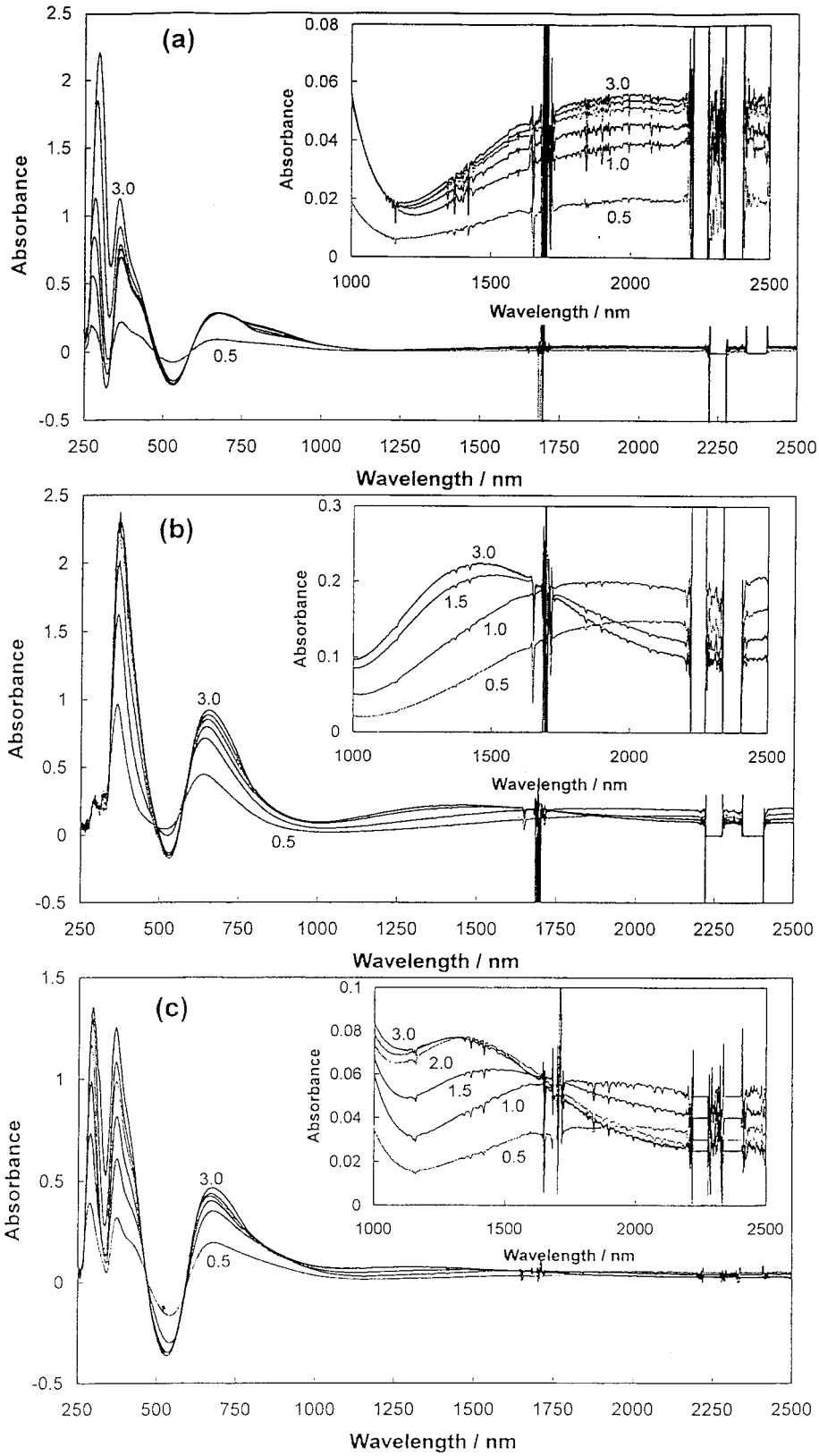

Figure 5. Differences in UV−vis−NIR absorption spectra of **1** (a), **2** (b), and **3** (c) in CH_2Cl_2 from the spectra of their neutral forms when they were oxidized by $[Fe(\eta^5\text{-}C_5H_4Cl)_2]PF_6$. The mole ratios of the oxidant to azo-bridged ferrocenes are 0.5, 1.0, 1.5, 2.0, 2.5, and 3.0, which are given as numbers in the figure.

acid, followed by the addition of NH_4PF_6. Ferrocene and BuLi−hexane solutions were obtained from Kanto Chemicals. Dinitrogen oxide (N_2O) (purity: 99.999%) was obtained from Sumitomo Precision Products. Bu_4NClO_4 and Bu_4NPF_6 were supplied from Tomiyama Chemicals as lithium battery grade. Anhydrous solvents used for the synthetic experiments were obtained from Kanto Chemicals. Acetone, acetonitrile, and dichloromethane used for the electrochemical and spectroscopic measurements were obtained from Kanto chemicals as an HPLC grade and were used as received. Nitrobenzene, nitromethane, 1,2-dichloroethane acetone (Kanto Chemicals, a guaranteed grade), and benzonitrile (Tokyo Kasei Chemicals, a guaranteed grade) were dried with 4 Å molecular sieves and used for the measurements. THF was distilled

Table 4. Parameters of IT Band for Azo-Bridged Ferrocene Oligomers[a]

		IT band					LMCT band	
complex	solvent	ν_{max}/cm^{-1}	ϵ/M^{-1} cm^{-1}	$\Delta\nu_{1/2}$/cm^{-1}	$10^2\alpha$	H_{AB}	ν_{max}/cm^{-1}	ϵ/M^{-1} cm^{-1}
$\mathbf{1}^+$	CH_2Cl_2	4911	368	4770	5.71	280	14880	1890
	DCE	5065	261	3690	4.17	211	14710	2550
	NM	6263	420	4520	5.27	330	15430	2620
	NB	5657	443	4470	5.67	321	15110	2670
	PhCN	5705	318	4510	4.80	274	15150	1650
	MeCN	6414	245	4700	4.06	260	15290	1360
	acetone	6380	358	4240	4.67	298	15430	2310
$\mathbf{2}^+$	CH_2Cl_2	4905	743	4610	10.6	520	15580	2710
	DCE	4567	986	4330	12.3	562	15770	3190
	NM	5890	744	4170	9.20	542	16450	2360
	NB	5731	866	4350	10.3	590	15970	2660
	PhCN	5537	824	4205	10.0	554	16080	2460
	MeCN	5967	560	3647	7.40	442	15970	1470
	acetone	5985	698	4060	8.70	521	16230	2110
	THF	6156	775	4060	9.10	560	16610	2660
$\mathbf{2}^{2+}$	CH_2Cl_2	6866	770	3950	–	–	15340	3030
	DCE	6770	962	3870	–	–	15290	3730
	NM	7212	958	3870	–	–	15580	3710
	NB	6711	969	3830	–	–	15240	3550
	PhCN	10350[b]	–	–	–	–	15150	1000
	MeCN	10640[b]	–	–	–	–	15580	1020
	acetone	7185	720	4300	–	–	15530	2920
	THF	7366	893	4330	–	–	15720	3510
$\mathbf{3}^+$	CH_2Cl_2	5623	474	4720	6.04	340	14750	2990
	THF	7200	410	4638	4.92	354	15340	3080
$\mathbf{3}^{2+}$	CH_2Cl_2	7460	512	4560	–	–	14970	2850
	THF	8139	427	4250	–	–	15290	2780

[a] Measurements were carried out for **1** [(1.3−2.5) × 10^{-4} M], **2** [(0.5−2.7) × 10^{-4} M], and **3** [(1.2−1.4) × 10^{-4} M] at 25 °C. α and H_{AB} for $\mathbf{2}^+$ and $\mathbf{3}^+$ were evaluated using 6.8 Å of the Fe−Fe distance as well as $\mathbf{1}^+$. [b] The band may not be the IT band (see text).

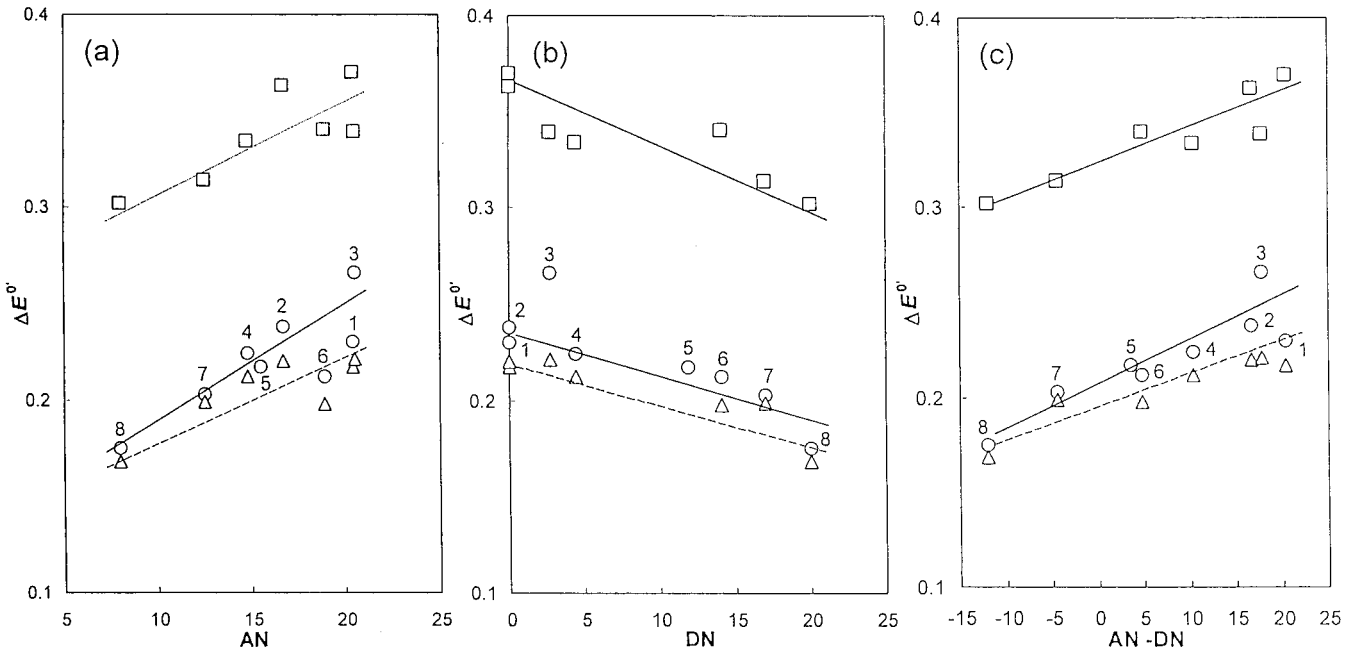

Figure 6. Plots of $\Delta E^{\circ\prime}$ vs AN (a), DN (b), or AN−DN (c) of solvents for **1** (○) and **2** (△, $\Delta E^{\circ\prime}_{12}$; □, $\Delta E^{\circ\prime}_{23}$). (1) CH_2Cl_2; (2) 1,2-dichloroethane (DCE); (3) nitromethane (NM); (4) nitrobenzene (NB); (5) PhCN; (6) MeCN; (7) acetone; (8) THF.

from Na-benzophenon ketyl under nitrogen prior to use. IR, UV−vis−NIR, ^{1}H NMR, and electron impact (EI) mass spectra were recorded with JASCO FT-IR 620V, JASCO V-570, JEOL GX400, and HITACHI M-80B spectrometers, respectively.

Synthesis of Azo-Bridged Ferrocene Trimers, 2 and 3. To a stirred solution of ferrocene (1.00 g, 5.4 mmol) in diethyl ether (20 mL) − THF (10 mL) cooled in an ice bath was added dropwise to a 1.64 M BuLi−hexane solution (5.0 mL, 8.2 mmol) under nitrogen. After the addition was completed, the solution was stirred for 1 h at room temperature and allowed to stand for 12 h. The resulting orange solution was cooled to −20 °C, to which N_2O gas was introduced by moderate bubbling for 30 min. The color of the solution changed to brown. The temperature of the solution was slowly raised to room temperature with stirring, causing a color change to purple, and then stirred at room temperature for 12 h. After evaporation, the residue was extracted with chloroform (500 mL), and the extract was washed with water (200 mL × 4) and dried with sodium sulfate. After filtration, chloroform was evaporated off to give a dark purple powdery residue. Silica gel column chromatography of this residue using chloroform as an eluent gave two purple bands besides a band of ferrocene and a broad band with

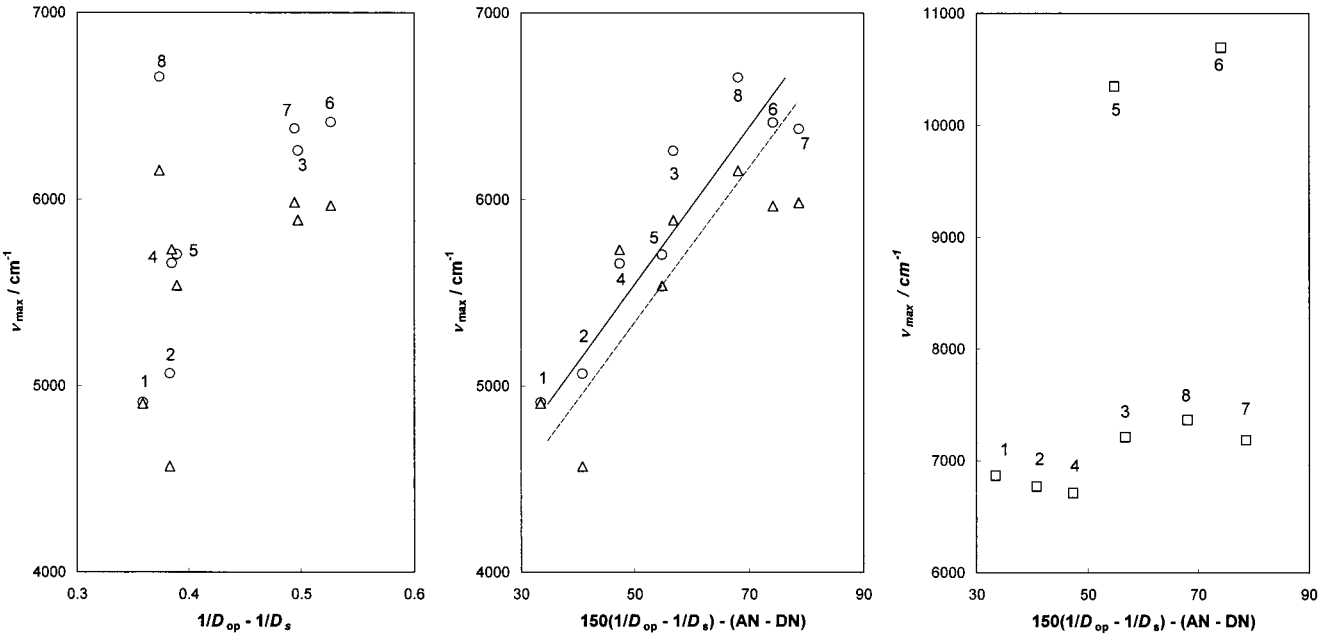

Figure 7. Plots of ν_{max} vs $(1/D_{op} - 1/D_s)$ (a) or $\{150(1/D_{op} - 1/D_s) - (AN-DN)\}$ (b, c) for $\mathbf{1}^+$ (○), $\mathbf{2}^+$ (△), and $\mathbf{2}^{2+}$ (□). Solvent numbers are the same as those given in Figure 6.

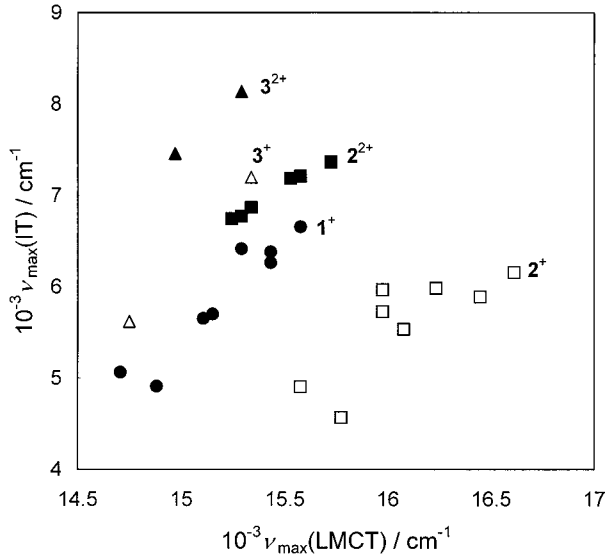

Figure 8. Plots of ν_{max}(IT) vs ν_{max}(LMCT) for mixed-valence states of **1**−**3**.

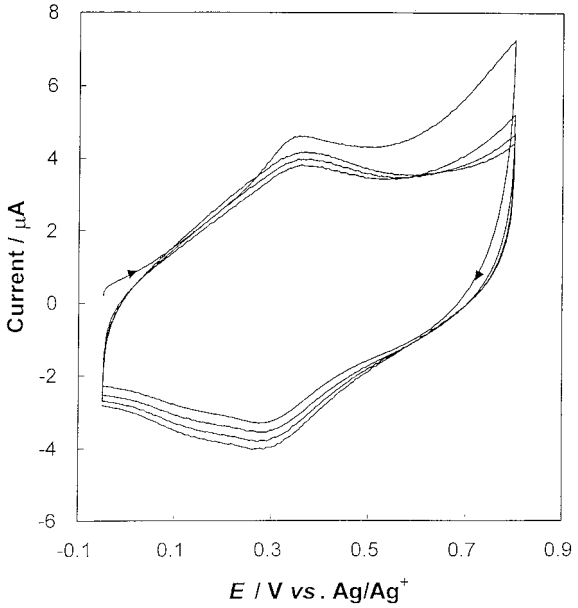

Figure 9. Cyclic voltammograms of **4** at GC in 0.1 M Bu_4NClO_4−CH_2Cl_2 at 0.1 V s^{-1}.

low R_f, probably due to higher molecular weight oligomers. The components obtained from the two purple bands were separated into single components using a JAI LC-908 recycling HPLC apparatus with JAIGEL-2H and JAIGEL-3H columns. **1** (yield: 74 mg, 6.9%) and **2** (yield: 58 mg, 5.6%) were obtained from the first band, and **3** (yield: 45 mg, 4.2%) was obtained from the second band.

Data for 2. ^{1}H NMR ($CDCl_3$): δ 4.89 (t, 2H, J = 2.0 Hz), 4.75 (t, 2H, J = 2.0 Hz), 4.48 (t, 2H, J = 2.0 Hz), 4.39 (t, 2H, J = 2.0 Hz), 4.32 (t, 2H, J = 2.0 Hz), 4.29 (t, 2H, J = 2.0 Hz), 4.25 (t, 2H, J = 2.0 Hz), 4.24 (s, 5H), 4.14 (t, 2H, J = 2.0 Hz) 3.98 (s, 5H) ppm. ^{13}C NMR ($CDCl_3$): δ 108.02, 107.94, 86.24, 82.35, 71.19, 69.74, 69.52, 69.36, 69.17, 67.94, 67.82, 66.62, 65.13, 64.16 ppm. MS-EI: m/z 582 (M^+). IR (KBr disk): 1445 ($\nu_{N=N}$), 1205 (ν_{C-N}) cm^{-1}. UV−vis ($CHCl_3$) λ_{max} (nm) 242 (ϵ = 17 810 M^{-1} cm^{-1}), 318 (ϵ = 17 160), 400 (sh, ϵ = 4550), 535 (ϵ = 4750). Anal. Calcd for $C_{30}H_{26}N_2Fe_3$: C, 61.90; H, 4.50; N, 4.81. Found: C, 61.97; H, 4.62; N, 4.87.

Data for 3. ^{1}H NMR ($CDCl_3$): δ 4.94 (t, 8H, J = 2.0 Hz), 4.54 (t, 4H, J = 2.0 Hz), 4.52 (t, 4H, J = 2.0 Hz), 4.30 (s, 10H). ^{13}C NMR ($CDCl_3$): δ 109.19, 107.81, 71.06, 69.88, 69.75, 65.43, 64.38 ppm. MS-EI: m/z 610 (M^+); IR (KBr disk): 1448 ($\nu_{N=N}$), 1210 (ν_{C-N}) cm^{-1}. UV−vis ($CHCl_3$) λ_{max} (nm) 241 (ϵ = 22 230), 322 (ϵ = 19 380), 400 (sh, ϵ = 6790), 542 (ϵ = 6790). Anal. Calcd for $C_{30}H_{26}N_4Fe_3$: C, 59.06; H, 4.30; N, 9.18. Found: C, 59.29; H, 4.60; N, 8.90.

Synthesis of Azo-Bridged Ferrocene Polymer (4). 1,1′-Dilithioferrocene was prepared by a reaction of ferrocene (0.49 g, 2.6 mmol) and 1.47 M BuLi−hexane solution (3.9 mL, 5.7 mmol) in the presence of tetramethylethylenediamine (TMEDA) (0.88 mL, 5.7 mmol) in hexane (30 mL) for 2 h. After the solution was allowed to stand overnight, the precipitate was separated by filtration, washed with hexane, and dissolved in THF (15 mL). The THF solution was transferred to a 100-mL autoclave and cooled in a liquid N_2 bath. N_2O gas (30 L at room temperature) was introduced, and the temperature of the mixture was gradually raised to room temperature with mechanical stirring. The pressure at room temperature was 40 kgf cm^2. The solution was stirred for 17 h at room temperature. The products obtained were dissolved in chloroform and filtered. The soluble products in chloroform were separated into polymeric and oligomeric components using a JAI LC-908 recycling HPLC apparatus with JAIGEL-2H and

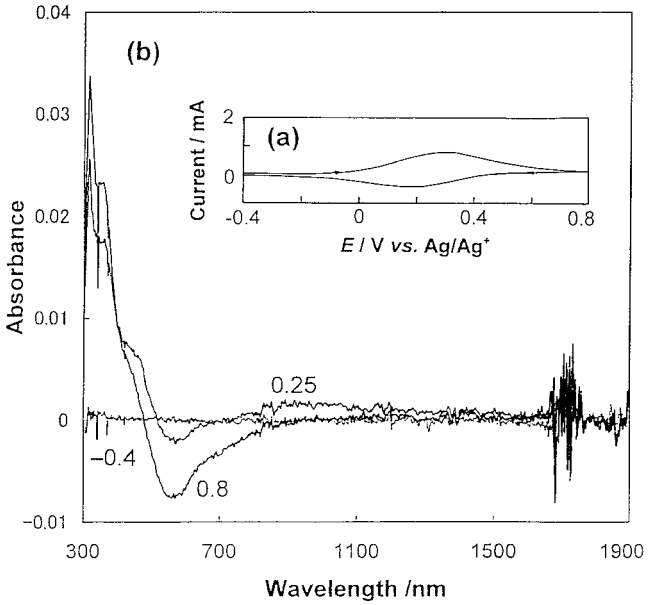

Figure 10. Cyclic voltammograms of a spin-coated film of **4** at ITO in 0.1 M Bu_4NClO_4−MeCN at 0.1 V s^{-1} (a), and the differences in the VIS−NIR spectra of the film at given potentials from the spectrum at −0.4 V vs Ag/Ag^+ (b). Numbers in the figure refer to the potential vs Ag/Ag^+.

JAIGEL-3H columns. The polymeric components for which the molecular weights were more than 3×10^3 based on the polystyrene standard were collected, and reprecipitation from chloroform−acetonitrile gave a polymer, **4**, in a yield of 0.21 g. ^{1}H NMR ($CDCl_3$): δ 3.8−4.6 (br, m). UV−vis ($CHCl_3$): λ_{max} (nm) 307 ($\epsilon' = \epsilon$/number of ferrocene units = 5210 M^{-1} cm^{-1}), 380 (ϵ = 3660), 535 (ϵ = 1680). Anal. Calcd for $C_{10}H_8N_{1.18}Fe$ ($(C_{10}H_8FeN_2)_{0.59}(C_{10}H_8Fe)_{0.41}$): C, 59.89; H, 4.02; N, 8.24. Found: C, 56.14; H, 5.20; N, 7.73.

Electrochemical Measurements. A glassy carbon rod (outside diameter 3 mm. Tokai Carbon GC-20) was embedded in Pyrex glass, and a cross-section was used as a working electrode. Cyclic voltammetry and Osteryoung square-wave voltammetry were carried out in a standard one-compartment cell under an argon atmosphere equipped with a platinum-wire counter electrode and an Ag/Ag^+ reference electrode (10 mM $AgClO_4$ in 0.1 M Bu_4NClO_4-MeCN, $E^{o'}$(ferrocene/ferrocenium in 0.1 M Bu_4NClO_4/CH_2Cl_2) = 0.214 V vs Ag/Ag^+) with a BAS CV-50W voltammetric analyzer. DigiSim2 (BAS) computer software was used for the simulation of a cyclic voltammogram. As for the polymer **4**, electrochemical measurements were also carried out for a spin-coated film on ITO.

Analysis of IT Bands in the Mixed-Valence States. A 10 mm × 10 mm quartz cell was connected to a Pyrex glass tube with six branched spaces to keep the oxidizing material and was used for the spectroscopic measurements. Setup of the samples in the cell was carried out in an argon-filled drybox. A given volume of an acetone solution of $[Fe(\eta^5\text{-}C_5H_4Cl)_2]PF_6$ was put in each branch of the cell, and the solvent was carefully evaporated to [leave a]solid residue. A solution of **1**, **2**, or **3** was put in the cell; the cell was then closed with a stopcock and placed outside of the drybox, and the spectrum was measured before and after the sample solution was mixed stepwise with the oxidant in six branches. This manipulation was repeated to give a series of successive changes with the amount of oxidant in the spectrum of each oligomer.

X-ray Structure Determination of 1. A crystal (0.10 × 0.30 × 0.40 mm) was mounted in a glass capillary, and data were collected at 296 K (Rigaku AFC5R diffractometer with graphite monochromated Mo Kα radiation (λ = 0.7107 Å) and a rotating anode generator). Crystal data: $C_{20}H_{18}Fe_2N_2$, M_r = 398.07, monoclinic, space group $P2_1/c$ (No. 14), a = 10.516(2) Å, b = 7.501(1) Å, c = 20.919(2) Å, β = 101.702(10)°, V = 1615.9(4) Å^3, Z = 4, ρ_{calc} = 1.636 g cm^{-3}, of 4205 reflections ($6 < 2\theta < 55°$), 3995 were unique. After Lorentz and polarization corrections, the structure was solved by direct methods and expanded using Fourier techniques. The non-hydrogen atoms were refined anisotopically. The final cycle of full-matrix least-squares refinement was based on 1782 observed reflections ($I > 3\sigma(I)$) and 240 valuable parameters, and it converged (largest parameter shift was 0.27 times its esd) with unweighted and weighted agreement factors of R = 0.058, R_w = 0.065. All calculations were performed using the teXsan crystallographic software package of Molecular Structure Corporation. A detailed description of the structure and its determination is provided in the Supporting Information.

Acknowledgment. This research was partly supported by Grants-in-Aid for Scientific Research (No. 09238101, No. 11136027, and No. 11309003) from the Ministry of Education, Science, Sports, and Culture, Japan, and The Asahi Glass Foundation.

Supporting Information Available: Tables of crystal data, structure solution and refinement, atomic coordinates, bond lengths and angles, and anisotropic thermal parameters for **1**. This material is available free of charge via the Internet at http://pubs.acs.org.

IC990646W